Journal of Molecular Structure xxx (xxxx) xxx

Contents lists available at ScienceDirect

Journal of Molecular Structure

journal homepage: www.elsevier.com/locate/molstr

Analysis of supramolecular interactions directing crystal packing of a *trans,trans,trans*-[diaquabis(4-quinolin-3-yl)-4*H*-1,2,4-triazole) *bis*(tricyanomethanide)iron(II)] complex: A combination of XRD, MEP, NBO, QTAIM, and NCI analyses

Zouaoui Setifi[a,b], Néstor Cubillán[c], Christopher Glidewell[d], Susanta K. Nayak[e], Miguel Morales-Toyo[f], Ruhollah Khajavian[g], Fatima Setifi[a,*], Masoud Mirzaei[g,*]

[a] *Laboratoire de Chimie, Ingénierie Moléculaire et Nanostructures (LCIMN), Université Ferhat Abbas Sétif 1, Sétif 19000, Algeria*
[b] *Département de Technologie, Faculté de Technologie, Université 20 Août 1955-Skikda, Skikda 21000, Algeria*
[c] *Programa de Química, Facultad de Ciencias Básicas, Universidad del Atlántico, Barranquilla, Colombia*
[d] *School of Chemistry, University of St Andrews, St Andrews, Fife, KY16 9ST, United Kingdom*
[e] *Department of Chemistry, Visvesvaraya National Institute of Technology, Nagpur, 440010, Maharashtra, India*
[f] *Facultad de Ciencias y Humanidades, Escuela de Educación, Universidad Central del Este (UCE), San Pedro de Macorís, 21000, Dominican Republic*
[g] *Department of Chemistry, Faculty of Science, Ferdowsi University of Mashhad, Mashhad 9177948974, Iran*

ARTICLE INFO

Article history:
Received 23 August 2020
Revised 8 October 2020
Accepted 9 October 2020
Available online xxx

Keywords:
Iron(II)
Polynitrile
Solvothermal
Crystal structure
Non-covalent interactions

ABSTRACT

The synthesis and structural characterization of a hydrated high-spin iron(II) complex [Fe(4-qtrz)$_2$(tcm)$_2$(H$_2$O)$_2$] are reported where 4-qtrz = 4-quinolin-3-yl-4*H*-1,2,4-triazole and tcm = tricyanomethide. The complex was prepared solvothermally and crystallizes in the triclinic space group $P\bar{1}$ with $Z = 1$, $a = 8.5221(3)$ Å, $b = 8.9343(5)$ Å, $c = 10.0081(5)$ Å, $\alpha = 85.147(2)°$, $\beta = 77.166(2)°$, $\gamma = 83.784(2)°$. The complex is centrosymmetric, with mutually trans pairs of water molecules, of tcm, and monodentate 4-qtrz coordinated via the triazole unit and a combination of O–H···N and C–H···N hydrogen bonds, forming a three-dimensional framework structure in which the shortest Fe···Fe distance is 8.5221(3) Å. An analysis of non-covalent interactions was conducted through reduced density gradient, quantum theory of atoms in molecules and natural bond orbitals. Accordingly, the important contributions of several intra- and inter-molecular hydrogen bonds stabilize the supramolecular structure. The hydrogen bonds occur by electron transfer from the tricyanomethanide nitrogen lone pairs to σ^* orbitals in the triazole, quinoline and water moieties. Other hydrogen bonds are attributed to π(CN) $\rightarrow$ σ^*, in triazole and quinoline, transfer. Additionally, a set of $\pi\cdots\pi^*$ interactions between cyano groups (CN···CN), π(phenyl of quinoline)···π^*(CN), and π[CC of C(CN)$_3$] to π^*(phenyl of quinoline) were also observed.

1. Introduction

Polynitrile anions have recently received much attention in the fields of coordination chemistry and molecular materials [1-7]. These organic anions are of interest for their ability to link metal ions in a variety of different ways either functioning alone or in combination with neutral co-ligands, provide opportunities for the generation of molecular architectures with varying dimensions and topologies [8-15].

Quantum Chemistry methods have gained popularity as a complement to crystallographic studies, allowing the in-depth exploration of intermolecular interactions in crystals [16-21]. Quantum theory of atoms in molecules (QTAIM) and the Reduced Density Gradient (RDG) are commonly used in discovery and explaining weak interactions. QTAIM study the topology of electron density encoding the information in the critical points. It have been important in identifying unconventional interactions, e.g. Dutta et al., characterized an unlikely parallel CN···CN interaction in [Cu(3-CNpy)(PDC)(H$_2$O)$_2$] (3-CNpy: 3-cyanopyridine and PDC: 2,6-pyridinedicarboxylate) [22].

On the other hand, the RDG – in simultaneous plotting with signed density – locates the non-covalent interactions in the molecular real-space by using mapped isosurfaces [23,24]. These plots, called NCI plots, permit the classification by relative strength and the identification of atom participating in the interactions.

* Corresponding authors.
E-mail addresses: fat_setifi@yahoo.fr (F. Setifi), mirzaeesh@um.ac.ir (M. Mirzaei).

https://doi.org/10.1016/j.molstruc.2020.129438
0022-2860/

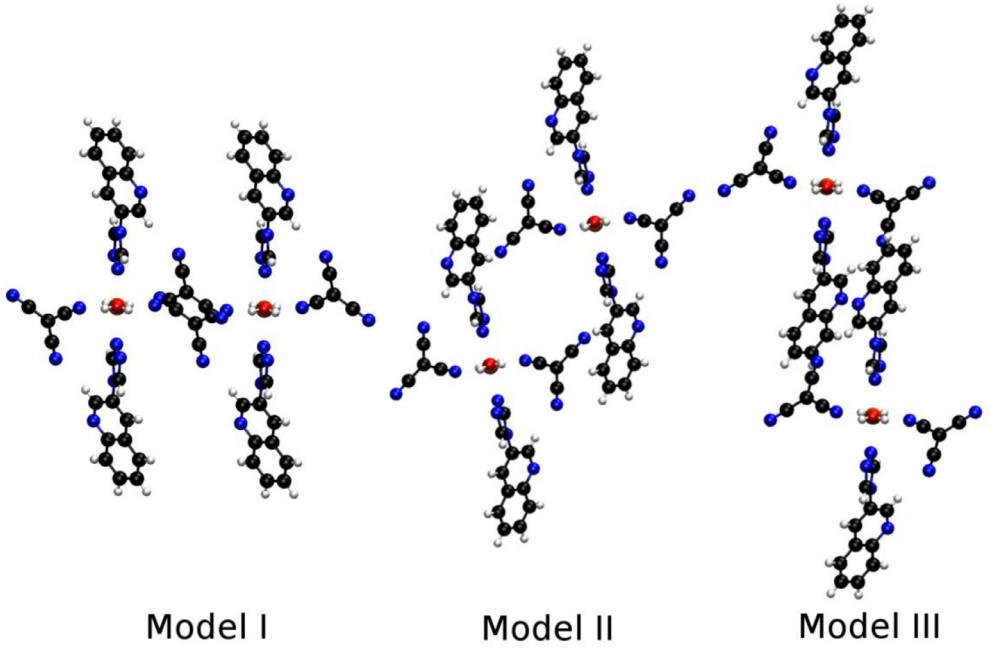

Fig. 1. Structure of molecular models for calculations. Model I: Dimer with intra- and intermolecular hydrogen bonds and CN···CN interaction; Model II: Dimer with intra- and intermolecular hydrogen bonds; Model III: Dimer with $\pi\cdots\pi$ interactions.

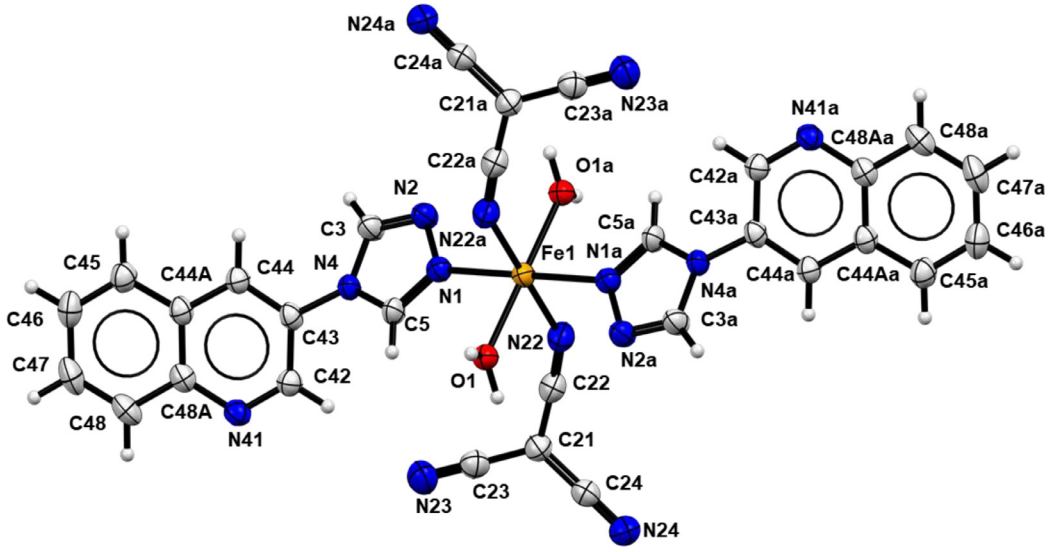

Fig. 2. The molecular structure of **1**, showing the atom-labeling scheme. Displacement ellipsoids are drawn at 50% probability level, and the atoms marked 'a' are at the symmetry position (1-*x*, 1-*y*, 1-*z*). Leading dimensions (Å, °): Fe1–N1, 2.1652(15); Fe1–N22, 2.1740(17); Fe1–O1, 2.0888(14); N1–Fe1–N22, 86.74(6); N1–Fe1–O1, 87.17(6); N22–Fe1–O1, 87.26(6).

The combination of these methods with X-ray crystallography have been important in identifying the basis of supramolecular structures, e.g. Hernandez-Paredes found the role of C–H···O interaction in the assembly of 5–methoxy–2-nitroaniline and its co-crystal with 2-amino-5-nitropyridine [25].

Herein, we report the successful synthesis and X-ray crystal structure characterization of an iron(II) complex bearing tcm and 4-qtrz ligands (tcm = tricyanomethide and 4-qtrz = 4-quinolin-3-yl-4*H*-1,2,4-triazole). High level theoretical and crystallographic studies demonstrate that $[Fe(4\text{-qtrz})_2(tcm)_2(H_2O)_2]$ (**1**) complex creates a three-dimensional structure mainly due to the ability of (tcm) anion in forming various non-covalent interactions.

2. Experimental

2.1. Materials and physical measurements

Organic starting compounds, iron salt, and solvents were purchased from commercial sources (analytical reagent grade) and used without further purification.

Elemental analyses (C, H and N) were performed using a Perkin-Elmer 2400 series II CHN analyzer. Infrared spectra were recorded in the range 4000–500 cm^{-1} on a FT-IR Bruker ATR Vertex 70 Spectrometer.

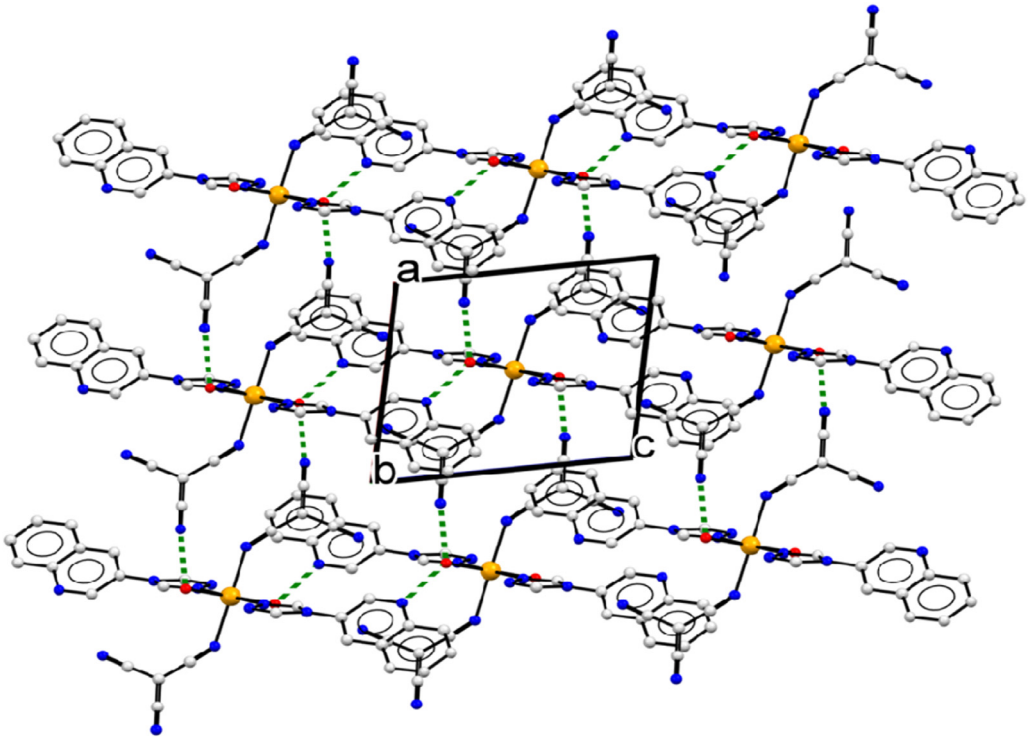

Fig. 3. A projection down [010] of part of the crystal structure of **1** showing the formation of a sheet built from O–H···N hydrogen bonds and lying parallel to (010). Hydrogen bonds are drawn as dashed lines and, for the sake of clarity, the H atoms bonded to C atoms have been omitted.

2.2. Synthesis

1 was prepared solvothermaly under autogenous pressure from a mixture of $FeSO_4{\cdot}7H_2O$ (55.6 mg, 0.2 mmol), 4-qtrz (39.24 mg; 0.2 mmol) and Ktcm (51.67 mg, 0.4 mmol) in H_2O/MeOH (4:1 v/v, 20 mL). This mixture was sealed in a Teflon-lined autoclave and heated at 160 °C for 2 days. After cooling to room temperature at a rate of 10 °C h^{-1}, red crystals were obtained containing **1**. Anal. Calc. (%) for $C_{30}H_{20}FeN_{14}O_2$ (664.45 g/mol): C, 54.23; H, 3.03; N, 29.51. Found: C, 54.17; H, 3.14; N, 29.32%. Main IR bands (ATR-IR, cm^{-1}): $\nu_{(CN)}$: 2187(s).

2.3. X-ray crystallography

Suitable single crystals of **1** were chosen for an X-ray diffraction study. Crystallographic measurements were collected at 100 K with a Bruker APEXII CCD diffractometer, using graphite-monochromatised Mo *Kα* (λ = 0.71073 Å) radiation. Data collection, cell refinement and data reduction were performed using APEX2 and absorption correction with SADABS [26]. The structure was solved by direct methods using SHELXS-97 [27] and refined by full-matrix least squares on F^2 with all data, using SHELXL-2014 [27]. All H atoms were located in difference maps. The H atoms bonded to C atoms were then treated as riding atoms in geometrically idealised positions with C–H distances 0.95 Å and with $U_{iso}(H) = 1.2\ U_{eq}(C)$. For the H atoms in the water ligand, the atomic coordinates were refined with $U_{iso}(H) = 1.5\ U_{eq}(O)$, giving O–H distances of 0.82(3) Å and 0.88(3) Å. Crystallographic data and details of the data collection and structure solution and refinements are listed in Table 1.

3. Computational details

The intra- and intermolecular interactions in the crystal structure were analyzed by studying the RDG, QTAIM, and Natural Bonds Orbitals (NBO). The RDG calculations were performed with NCIPlot 3.0 using the densities obtained through Unrestricted Open Shell Density Functional Theory (DFT) calculations [23,24]. All calculations DFT and NBO calculations were carried-out at the level with UM06–2X and 6–311G** basis set with Gaussian 09 Rev. A.02 [28]. QTAIM calculation were realized with Multiwfn 3.6 [29]. All isosurfaces and QTAIM molecular graphs were performed with VMD [30].

Three molecular models were built by dimers representing the inter- and intra-molecular interactions in the crystal (Models I-III in Fig. 1). In these models, the density was extracted from single-point calculations. Additionally, the geometry of the isolated molecule was optimized and the absence of negative eigenvalues in hessian matrix confirmed by a vibrational analysis. Unrestricted open shell and restricted open shell calculations were carried-out on this molecule in order to compare the electronic structure of this high-spin complex.

4. Results and discussion

4.1. Synthesis and characterization

The starting salt Ktcm and the 4-qtrz ligand were synthetized and characterized, and further used in the synthesis of the title complex. The IR spectrum of **1** exhibits strong absorption band at 2187 cm^{-1} ascribed to the ν(CN) of the tcm anion. The value of this absorption band is slightly shifted to higher wave-numbers, corresponding to coordinated $(tcm)^-$ moieties [31].

Table 1
Crystal data and structure refinement parameters for **1**.

Chemical formula	$C_{30}H_{20}FeN_{14}O_2$
M_r	664.45
Crystal system, space group	Triclinic, $P\bar{1}$
Temperature (K)	100
a, *b*, *c* (Å)	8.5221 (3), 8.9343 (5), 10.0081 (5)
α, β, γ (°)	85.147 (2), 77.166 (2), 83.784 (2)
V (Å^3)	737.16 (6)
Z	1
Radiation type	Mo *Kα*
μ (mm^{-1})	0.57
Crystal size (mm)	0.32 × 0.26 × 0.17
Data collection	
Diffractometer	Bruker APEXII CCD
Absorption correction	Multi-scan (*SADABS*; Bruker, 2015)
T_{min}, T_{max}	0.686, 0.738
No. of measured, independent and observed [$I > 2\sigma(I)$] reflections	30759, 5354, 3877
R_{int}	0.116
$(\sin\theta/\lambda)_{max}$ (Å^{-1})	0.757
Refinement	
$R[F^2 > 2\sigma(F^2)]$, w$R(F^2)$, *S*	0.049, 0.138, 1.07
No. of reflections	5354
No. of parameters	220
H-atom treatment	H-atom parameters constrained
$\Delta\rho_{max}$, $\Delta\rho_{min}$ (e Å^{-3})	0.54, −0.81

4.2. Description of the crystal structure

The octahedral Fe(II) lies on a center of inversion, selected as that at (0.5, 0.5, 0.5), and it is coordinated by mutually *trans* pairs of 4-quinolin-3-yl-4*H*-1,2,4-triazole molecules, tricyanomethanide anions and water molecules. The monodentate quinolinyltriazole ligands coordinate *via* the triazole unit, rather than *via* the quinoline unit (Fig. 2). The all-*trans* configuration of this centrosymmetric complex means that the ligating atoms N1, N22 and O1 adopt a facial (*fac*) arrangement. The bond distances to Fe (Fig. 2) indicate the presence of a high spin configuration, since for a low-spin configuration, the bond distances to Fe would be clustered around 1.97 Å [32]. Within the quinolinyltriazole ligand, the two components make a dihedral angle of 39.52(6)°, the tricyanomethanide ligand is effectively planar, and its C–C distances are identical within experimental uncertainty, as are the C–N distances, indicating a uniform delocalization of the negative charge over all three cyano groups.

The supramolecular assembly is dominated by two O–H···N hydrogen bonds (Table 2), augmented by a number of C–H···N hydrogen bonds. The hydrogen bonds involving H1A links the complexes into a C(11) [33-35] chain running parallel to the [100] direction, within which the shortest Fe···Fe distance is 8.5221(3) Å, while that involving H1B links complexes related by inversion into cyclic, centrosymmetric dimers characterised by an $R_2^2(18)$ motif, and an Fe···Fe distance of 10.0081(5) Å. In combination, these two hydrogen bonds generate a complex sheet lying parallel to (010) (Fig. 3). Three of the C–H···N hydrogen bonds lie within this sheet, but that involving atom C44 as the donor links the sheets into a continuous three-dimensional array.

There is also a single C–N···π(arene) interactions, with dimensions N24···Cg1^{i} 3.880(2) Å, C24···Cg1^{i} 3.9887(19) Å and C24–N24···Cg1^{i} 86.90(13)°, where Cg1 represents the centroid of the quinolinyl ring (C44A, C45–C48,C48A) and the symmetry code *i* = (1-*x*, 1-*y*, 1-*z*). This interaction thus reinforces the hydrogen-bonded $R_2^2(18)$ ring described above (Fig. 4). However, there are no significant cyano···cyano interactions in this structure. Although there is a pair of anti-parallel, inversion-related cyano groups lying across the center of the hydrogen-bonded $R_2^2(18)$ ring (Fig. 4), the associated geometric parameters [N23···N23^{i} 3.994(3) Å, C23···N23^{i} 4.510(3) Å. And C23···C23^{i} 5.234(3) Å, where the

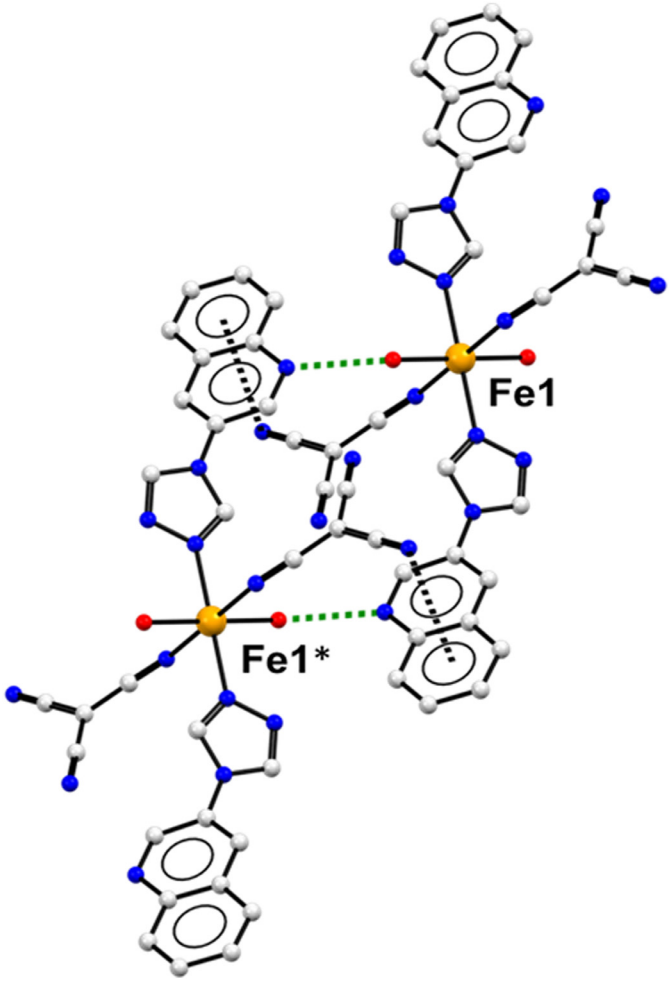

Fig. 4. Part of the crystal structure of compound (A) showing the C–N···π(arene) interaction within the hydrogen-bonded $R_2^2(18)$ ring. For the sake of clarity, the H atoms bonded to C atoms, and the unit-cell outline have been omitted. Hydrogen bonds and the N···ring interactions are drawn as dashed lines: the Fe atoms marked Fe1 and Fe1* are at (0.5, 0.5, 0.5) and (0.5, 0.5, −0.5) respectively.

Table 2
Hydrogen-bond geometry (Å, º) for **1**.

D–H···A	D–H	H···A	D···A	D–H···A	Symmetry
O1–H1A···N24	0.82(3)	2.02(3)	2.837(2)	179(3)	1 + *x*, *y*, *z*
O21–H1B···N41	0.88(3)	1.95(3)	2.817(2)	172(3)	1-*x*, 1-*y*, -*z*
C5–H5···N23	0.95	2.43	3.249(3)	145	1-*x*,1-*y*,-*z*
C42–H42···N23	0.95	2.51	3.454(3)	174	*x*,*y*,*z*
C44–H44···N24	0.95	2.41	3.297(3)	154	1 + *x*,−1 + *y*,*z*
C48–H48···N2	0.95	2.45	3.397(3)	175	*x*, *y*, −1 + *z*

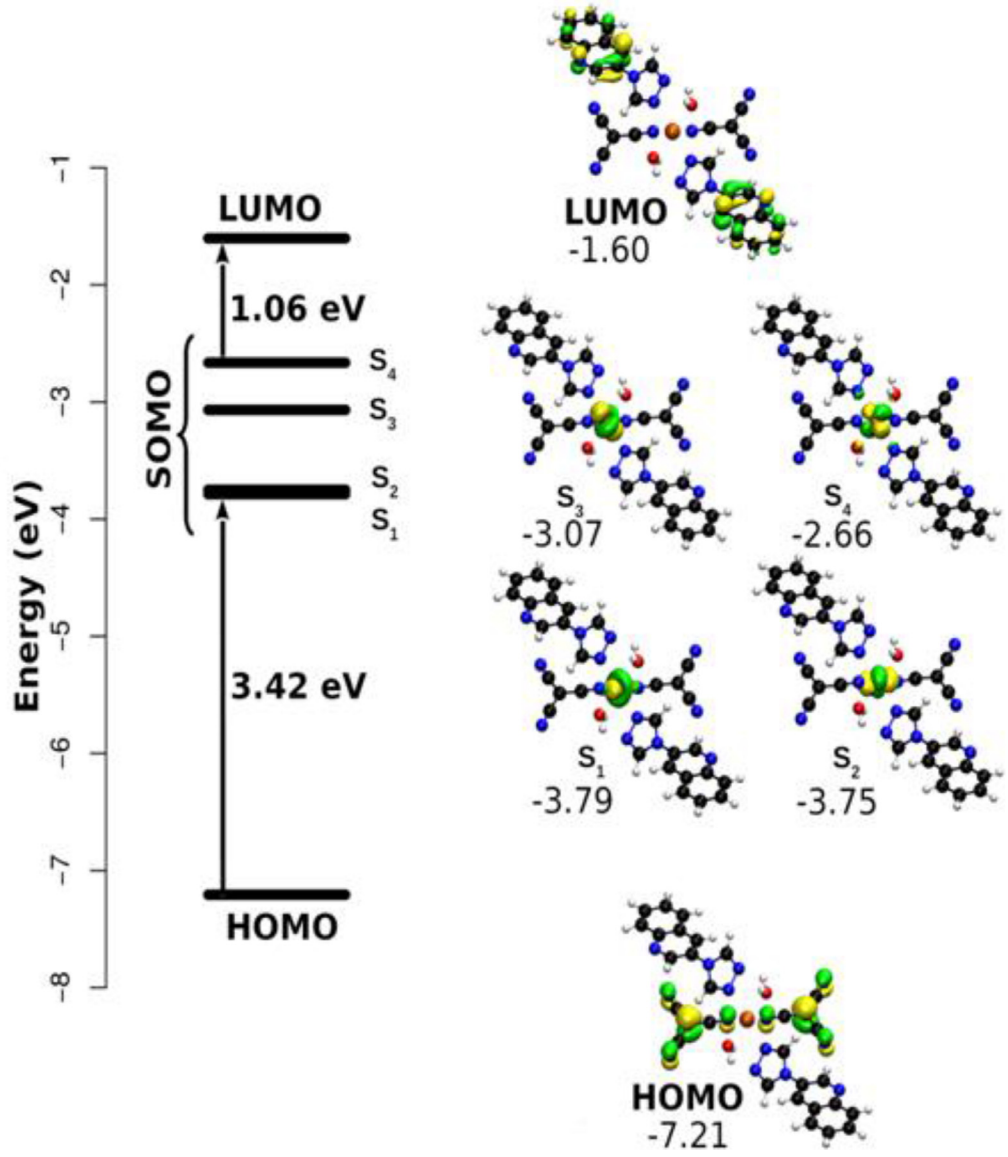

Fig. 5. Molecular frontier orbitals and energy levels diagram of **1**.

symmetry code i = (1-*x*, 1-*y*, -*z*)] indicate that the interaction energy between these two groups is likely to be negligibly small [36].

5. Molecular modeling

5.1. Isolated molecule

After the geometry optimization procedure, the structure of the isolated molecule was non-significantly modified, keeping the symmetry point group (c_i) and the majority of geometrical characteristics. In this sense, the electronic and magnetic properties can be interpreted in the light of frontier molecular orbitals. Fig. 5 shows the orbital diagram for the title compound as obtained by unrestricted and restricted open shell DFT calculations. The electrons in HOMO delocalize on both tricyanomethanide anions, while LUMO electrons are delocalized on the quinoline fragments. SOMOs are associated to *d* orbitals of Fe(II) (Fig. 5).

The HOMO-SOMO(S_1) and the SOMO(S_4)-LUMO gaps are 3.42 and 1.06 eV, respectively. These values show the feasibility of ligand-metal (trycianomethanide-iron(II)) and metal-ligand (iron(II)-quinoline fragments) electron transfer and, consequently, the redox properties of the metal. The spin density plots are given

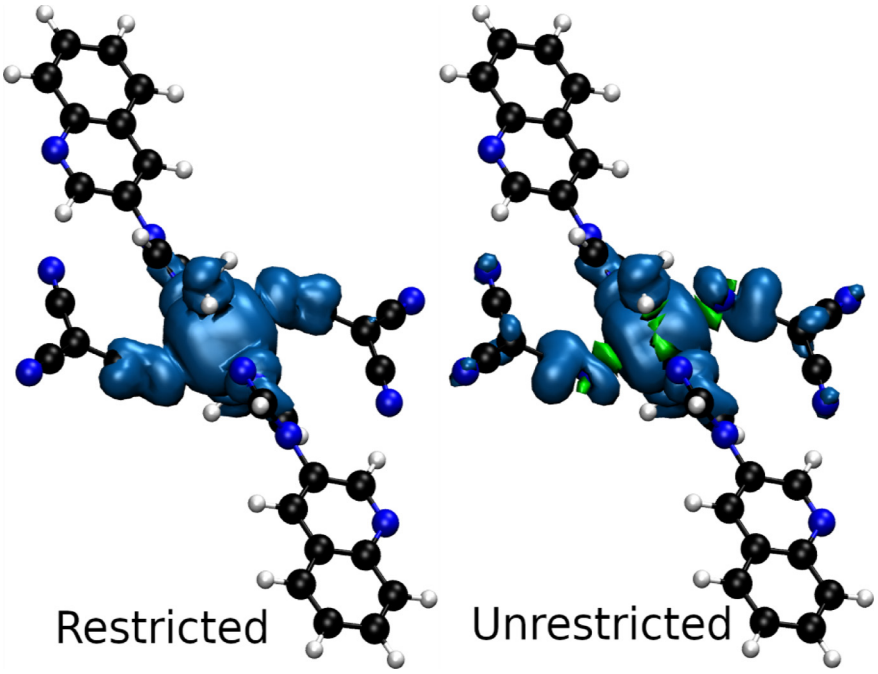

Fig. 6. Total spin density plot of **1**. Left Restricted open-shell Density Functional Theory; Right: Unrestricted open-shell Density Functional Theory.

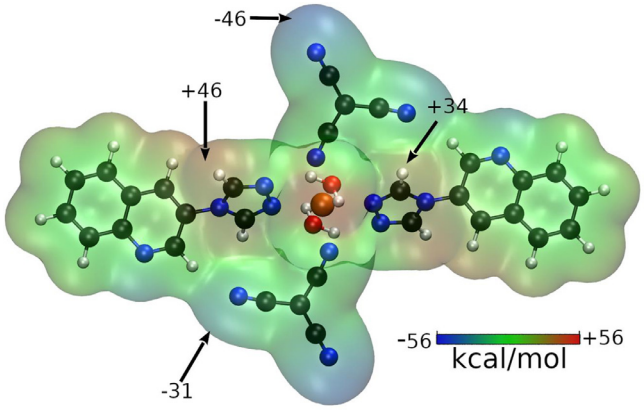

Fig. 7. Molecular electrostatic potential of **1** showing the extrema points.

in Fig. 6, showing the degree of delocalization of unpaired electrons condensed on the metal and the linking atoms of the ligands.

The rest of the charge distribution in the molecule is observed in the Molecular Electrostatic Potential (MEP) (Fig. 7). The maximum and minimum of MEP are located on the water ligands. The following extrema are mainly located on the hydrogen atoms of the triazole fragment (maxima) and the nitrogen atoms of the tricyanomethanide anion (minima). As will be shown, all of intra- and inter-molecular interactions are associated to these MEP's extrema.

5.2. Non-covalent interactions

Fig. 8 shows the RDG isosurface and QTAIM molecular graph of the Models I-III. We identified two intramolecular interactions involving hydrogens, labels B_1, and B_2 in Fig. 8, and linking the 4-quinolin-3-yl-4*H*-1,2,4-triazole ligand by the quinoline (B_1) and triazole (B_2) moieties, respectively. According to RDG vs sign(λ_2)ρ plot (Fig. S1), B_1 is located at −0.00832 au in sign(λ_2)ρ characterizing a weak interaction. The QTAIM values of critical point showed in Table 3 suggest a closed shell non-covalent interaction ($\nabla^2\rho > 0$ and $|V|/G < 1$ [37] involving symmetrical density ($\varepsilon \approx 0$). The NBO results of isolated molecule (optimized structure) support this observation showing that interaction as a charge transfer from the nitrogen lone-pair to the σ^*[0.6102·C(sp^2) – 0.7923·H(s)] with a second order perturbation energy, $E^{(2)}$, of 1.58 kcal/mol (0.25 kcal/mol for non-optimized geometry) (Table 3).

Table 3
QTAIM and NBO properties of the representative interactions in the models. Labels are the interactions showed in Fig. 8.

Label	ρ(au)	$\nabla^2\rho$(au)	|V|/G	ε	$E^{(2)}$ (kcal/mol)	Donor-acceptor transfer[a]
B1	0.00832	0.0273	0.752	0.0117	0.25/1.58[b]	$LP(N)_{tcm} \rightarrow \sigma^*(CH)_{qui}$
B2	0.00265	0.00829	0.723	0.310	<0.03/0.07[b]	$\pi(CN)_{tcm} \rightarrow \sigma^*(CH)_{trz}$
B3	0.0209	0.0876	0.828	0.0396	1.46	$LP(CN)_{tcm} \rightarrow \sigma^*(HO)_{H2O}$
B4	0.00460	0.0141	0.812	0.816	<0.03	$\pi(CN)_{tcm} \rightarrow \pi^*(CN)_{tcm}$
B5	0.00711	0.0236	0.775	0.0926	0.18	$LP(N)_{tcm} \rightarrow \sigma^*(CH)_{trz}$
B6	0.0105	0.0366	0.750	0.0509	0.25	$LP(CN)_{tcm} \rightarrow \sigma^*(CH)_{qui}$
B7	0.000967	0.00350	0.652	0.608	<0.03	$\pi(CN)_{tcm} \rightarrow \sigma^*(CH)_{qui}$
B8	0.00561	0.0156	0.793	2.20	0.10	$\pi(CC)_{pH} \rightarrow \pi^*(CN)_{tcm}$
B9	0.00540	0.0152	0.792	0.993	0.20	$\pi(CC)_{tcm} \rightarrow \pi^*(CC)_{ph}$

[a] cm: tricyanomethanide; qui: quinoline; trz: triazole; H_2O: water; pH: phenyl; LP: lone-pair.
[b] Values after slash are second order perturbation energy of geometry-optimized discrete unit.

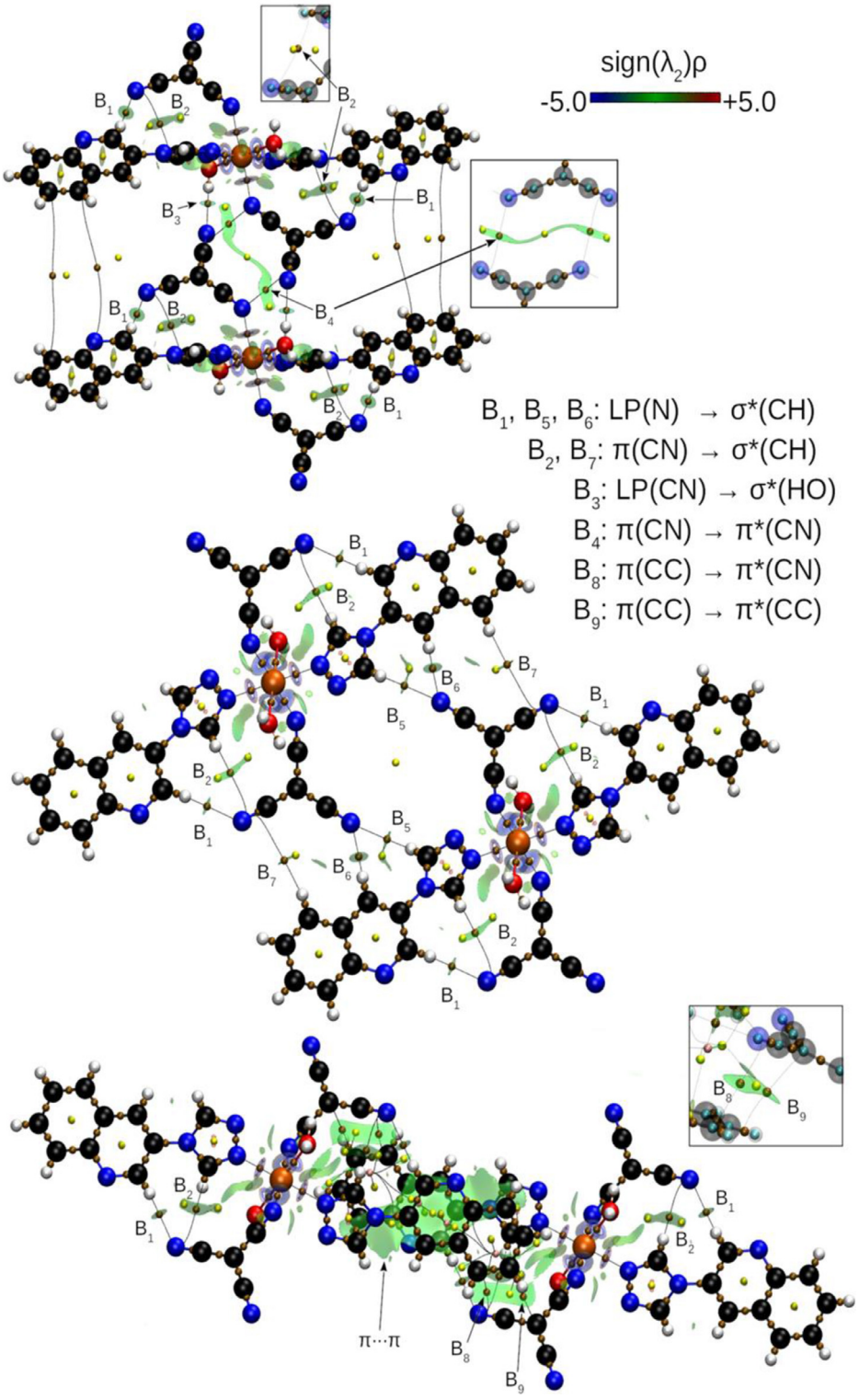

Fig. 8. NCI plot and QTAIM molecular graphs of models **I, II**, and **III** showing the representative intra- and inter-molecular interactions. Full NCI plots are shown in Figs. S1-S3.

The ρ (0.00265 au) and $\nabla^2\rho$ (0.00829 au) in B_2 are lower than the B_1. Similar to B_1, the $|V(r)|/G(r)$ ratio < 1. The value of ε (0.31 au) suggests a π contribution [38], which is confirmed by the NBO analysis. A charge transfer from π(CN) [0.6364 C(*sp*) + 0.7714 N(*sp*)] to the σ^*(CH) orbital and $E^{(2)}$ (0.07 kcal/mol, Table 1) was observed. According to Grabowski and Leszczynski, low values of ρ and $\nabla^2\rho$ imply long X–H$\cdots\pi$ distance and low $E^{(2)}$ [39].

Moreover, the presence of curvatures of the bond path near to both attractors related to B_2 (Fig. 7) are associated to structures near to catastrophe points, i.e. bond cleavage and/or formation [40]. Maley and Mawhinney [41] showed that the curvature is related to the C–S bond breaking in isothiirane. A similar result was reported by Nanayakkara and Kraka [42] for the isomerization of the HCN to CNH. Consequently,

all of these evidences suggest that B_2 is a weak C–H$\cdots\pi$ interaction.

The intermolecular interactions are four hydrogen bonds, CN$\cdots$CN, and $\pi\cdots\pi$ interaction. The interaction – labeled as B_3 – represents a hydrogen bond between the nitrogen of tricyanomethanide and the water ligand. There are relatively high values of ρ and $\nabla^2\rho$, and low value in ε (Table 3), suggesting a strong closed shell interaction and a cylindrical symmetry. The nature of the interaction is a charge transfer from nitrogen lone-pair of tricyanomethanide to the σ^*(OH) with the greatest second order perturbation energy (1.46 kcal/mol). Similarly, B_5 and B_6 are related to the interaction between the lone-pair of nitrogen and antibonding σ(CH) of triazole and quinoline fragments, respectively.

B_7 shows the lowest density and laplacian of density values, implying a weak interaction. The values ε close to one revealed a high contribution of π orbitals. The path curvature near to nitrogen confirmed the weakness of the interaction due to a catastrophe point in the vicinity of this structure. The characteristics of this critical point are similar to B_2, consequently, we can associate this interaction to a π(CN) $\rightarrow$ σ^*(CH) transfer.

The CN$\cdots$CN interaction, B_4, both nitriles have a quasi-parallel conformation – torsion angle of 49.5° This arrangement is not commonly observed in the literature [43]. The critical point associated to this interaction have ρ-value of 0.0046 au and ellipticity of 0.816. In the CN$\cdots$CN parallel configuration of [Cu(3-CNpy)(PDC)$(H_2O)_2$], Dutta et al. reported ρ-value of 0.0039 au at B3LYP-D/def2-TZVP level of theory [22]. In the other case, antiparallel configuration, it was reported 0.0553 au in ρ from experimental electron density for 2-methyl-4-nitro-1-phenyl-1*H*-imidazole-5-carbonitrile [44]. The intermediate value between the two extrema revealed the dipole-dipole nature of this interaction, as suggested by literature [43-45].

B_8 and B_9 are two interactions relating the tricyanomethanide ion with the phenyl portion of quinoline fragment (Fig. 8). The topological properties of these critical points are quite similar, indicating a closed shell interaction with a high asymmetry in the charge distribution along bond path. According to NBO results, these interactions are associated to $\pi \rightarrow \pi^*$ transfer. B_8 implies electron transfer from the π[0.7601 C(p) + 0.7801 C(p)] orbital of the phenyl portion of the quinoline towards the π^*[0.7667C(p) – 0.6427 N(p)] of the tricyanomethanide anion. On the other hand, the electron transfer in B9 is from orbital π[0.8729 C(p) + 0.4879 C(p)] of the tricyanomethanide to the π^*[0.7081 C(p) – 0.7061 C(p)] of phenyl ring.

Concluding remarks

In summary, synthesis, characterization, and supramolecular three-dimensional structure of a new centrosymmetric iron(II) complex formulated as $[Fe(4\text{-qtrz})_2(tcm)_2(H_2O)_2]$ is reported. The structural analysis shows that the environment around the six-coordinated Fe^{II} ion is octahedral and it presents the high spin configuration. The non-covalent interactions analysis by reduced density gradient, quantum theory of atoms in molecules and natural bond orbitals showed important contributions of several intra- and inter-molecular hydrogen bonds stabilizing the supramolecular structure. These hydrogen bonds are mainly associated to electron transfer from lone pairs on the nitrogen atoms of $C(CN)_3$ anion to σ^*(HC) and σ^*(HO) orbitals in the triazole, quinoline and water moieties of the complex. The rest of hydrogen bonds are attributed to $\pi(CN)_{tcm} \rightarrow \sigma^*$(CH from triazole or quinoline) transfer. Additionally, a set of $\pi\cdots\pi^*$ interactions between cyano groups (CN$\cdots$CN), π(phenyl of quinoline)$\cdots\pi^*$(CN), and π[CC of $C(CN)_3$] to π^*(phenyl of quinolone) were observed.

Authors' contributions

This paper has multiple authors and our individual contributions were as below

Statement (if applicable):

Zouaoui Setifi: Main idea, supervision, final writing the manuscript. Néstor Cubillán: Performed DFT studies. Christopher Glidewell: Crystallographer. Susanta K. Nayak: Experimental work performance, first-draft preparation. Miguel Morales-Toyo: Experimental work performance, first-draft preparation. Ruhollah Khajavian: Data analysis and first-draft preparation. Fatima Setifi: Co-supervision. Masoud Mirzaei: Main idea, supervision, final writing the manuscript.

Declaration of Competing Interest

There are no conflicts to declare.

Acknowledgements

Authors are indebted to the Algerian Ministère de l'Enseignement Supérieur et de la Recherche Scientifique (MESRS), the Direction Générale de la Recherche Scientifique et du Développement Technologique (DGRSDT) as well as the Université Ferhat Abbas Sétif 1 for financial support. M. M. gratefully acknowledges the financial support from the Ferdowsi University of Mashhad, Iran Science Elites Federation (ISEF), Zeolite and Porous Materials Committee of Iranian Chemical Society and the Iran National Science Foundation (INSF). M. M. also acknowledges the Cambridge Crystallographic Data center (CCDC) for access to the Cambridge Structural Database.

Supplementary materials

Supplementary material associated with this article can be found, in the online version, at doi:10.1016/j.molstruc.2020.129438.

References

[1] Y.S. Kayukov, S. Karpov, A. Grigor'ev, O. Nasakin, V. Tafeenko, K. Lyssenko, A. Shapovalov, E. Varaksina, Dalton Trans. 46 (2017) 16925–16938.
[2] Z. Setifi, F. Lehchili, F. Setifi, A. Beghidja, S.W. Ng, C. Glidewell, Acta Crystallogr. Sec. C 70 (2014) 338–341.
[3] A. Addala, M. Poupon, S. Bernès, G.S. Kürkçüoğlu, X. Liu, F. Lehchili, M. Kučeráková, M. Dušek, F. Setifi, Polyhedron 170 (2019) 271–277.
[4] A. Addala, F. Setifi, K.G. Kottrup, C. Glidewell, Z. Setifi, G. Smith, J. Reedijk, Polyhedron 87 (2015) 307–310.
[5] F. Lehchili, F. Setifi, X. Liu, A. Saneei, M. Kučeráková, Z. Setifi, M. Dušek, M. Poupon, M. Pourayoubi, J. Reedijk, Polyhedron 131 (2017) 27–33.
[6] F. Setifi, C. Charles, S. Houille, F. Thétiot, S. Triki, C.J. Gómez-García, S. Pillet, Polyhedron 61 (2013) 242–247.
[7] F. Setifi, D.K. Geiger, I. Abdul Razak, Z. Setifi, Acta Crystallogr. Sec. C 71 (2015) 658–663.
[8] C. Atmani, F. Setifi, S. Benmansour, S. Triki, M. Marchivie, J.-Y. Salaün, C.J. Gómez-García, Inorg Chem Commun 11 (2008) 921–924.
[9] S. Benmansour, C. Atmani, F. Setifi, S. Triki, M. Marchivie, C.J. Gómez-García, Coord Chem Rev 254 (2010) 1468–1478.
[10] S. Benmansour, F. Setifi, C.J. Gómez-García, S. Triki, E. Coronado, J.-Y. Salaün, J Mol Struct 890 (2008) 255–262.
[11] S. Benmansour, F. Setifi, S. Triki, C.J. Gómez-García, Inorg Chem 51 (2012) 2359–2365.
[12] S. Benmansour, F. Setifi, S. Triki, J.Y. Salaün, F. Vandevelde, J. Sala-Pala, C.J. Gómez-García, T. Roisnel, Eur J Inorg Chem 2007 (2007) 186–194.
[13] A.O. Dmitrienko, M.I. Buzin, Z. Setifi, F. Setifi, E.V. Alexandrov, E.D. Voronova, A.V. Vologzhanina, Dalton Trans. 49 (2020) 7084–7092.
[14] F. Setifi, S. Benmansour, M. Marchivie, G. Dupouy, S. Triki, J. Sala-Pala, J.-Y. Salaün, C.J. Gómez-García, S. Pillet, C. Lecomte, E. Ruiz, Inorg Chem 48 (2009) 1269–1271.
[15] F. Setifi, E. Milin, C. Charles, F. Thétiot, S. Triki, C.J. Gomez-Garcia, Inorg Chem 53 (2014) 97–104.
[16] M. Mirzaei, H. Eshtiagh-Hosseini, M. Alipour, A. Bauzá, J.T. Mague, M. Korabik, A. Frontera, Dalton Trans. 44 (2015) 8824–8832.
[17] M. Mirzaei, H. Eshtiagh-Hosseini, M. Bazargan, F. Mehrzad, M. Shahbazi, J.T. Mague, A. Bauzá, A. Frontera, Inorganica Chim Acta 438 (2015) 135–145.

[18] M. Mirzaei, H. Eshtiagh-Hosseini, Z. Karrabi, K. Molčanov, E. Eydizadeh, J.T. Mague, A. Bauzá, A. Frontera, CrystEngComm 16 (2014) 5352–5363.
[19] M. Mirzaei, H. Eshtiagh-Hosseini, N. Lotfian, A. Salimi, A. Bauzá, R. Van Deun, R. Decadt, M. Barceló-Oliver, A. Frontera, Dalton Trans. 43 (2014) 1906–1916.
[20] M. Mirzaei, H. Eshtiagh-Hosseini, M. Shamsipur, M. Saeedi, M. Ardalani, A. Bauzá, J.T. Mague, A. Frontera, M. Habibi, RSC Adv 5 (2015) 72923–72936.
[21] M. Mirzaei, H. Eshtiagh-Hosseini, S. Zarghami, A. Bauzá, A. Frontera, J.T. Mague, H. Morteza, M. Shamsipur, CrystEngComm 16 (2014) 1359–1377.
[22] D. Dutta, S.M. Nashre-ul-Islam, U. Saha, A. Frontera, M.K. Bhattacharyya, J Mol Struct 1195 (2019) 733–743.
[23] E.R. Johnson, S. Keinan, P. Mori-Sánchez, J. Contreras-García, A.J. Cohen, W. Yang, J. Am. Chem. Soc. 132 (2010) 6498–6506.
[24] J. Contreras-García, E.R. Johnson, S. Keinan, R. Chaudret, J.-.P. Piquemal, D.N. Beratan, W. Yang, J Chem Theory Comput 7 (2011) 625–632.
[25] J. Hernández-Paredes, R.C. Carrillo-Torres, A.A. López-Zavala, R.R. Sotelo–Mundo, O. Hernández-Negrete, J.Z. Ramírez, M.E. Alvarez-Ramos, J Mol Struct 1119 (2016) 505–516.
[26] Bruker, APEX2, SAINT, and SADABS, Bruker AXS Inc., Madison, Wisconsin, USA, 2015.
[27] G. Sheldrick, Acta Crystallogr. Sec. A 71 (2015) 3–8.
[28] M.J. Frisch, G.W. Trucks, H.B. Schlegel, G.E. Scuseria, M.A. Robb, J.R. Cheeseman, G. Scalmani, V. Barone, B. Mennucci, G.A. Petersson, H. Nakatsuji, M. Caricato, X. Li, H.P. Hratchian, A.F. Izmaylov, J. Bloino, G. Zheng, J.L. Sonnenberg, M. Hada, M. Ehara, K. Toyota, R. Fukuda, J. Hasegawa, M. Ishida, T. Nakajima, Y. Honda, O. Kitao, H. Nakai, T. Vreven, J.A. Montgomery, J.E. P Jr., F. Ogliaro, M. Bearpark, J.J. Heyd, E. Brothers, K.N. Kudin, V.N. Staroverov, R. Kobayashi, J. Normand, K. Raghavachari, A. Rendell, J.C. Burant, S.S. Iyengar, J. Tomasi, M. Cossi, N. Rega, J.M. Millam, M. Klene, J.E. Knox, J.B. Cross, V. Bakken, C. Adamo, J. Jaramillo, R. Gomperts, R.E. Stratmann, O. Yazyev, A.J. Austin, R. Cammi, C. Pomelli, J.W. Ochterski, R.L. Martin, K. Morokuma, V.G. Zakrzewski, G.A. Voth, P. Salvador, J.J. Dannenberg, S. Dapprich, A.D. Daniels, Ö. Farkas, J.B. Foresman, J.V. Ortiz, J. Cioslowski, D.J. Fox, Gaussian 09 Rev. D. 01, Gaussian, Inc., Wallingford CT, 2009.
[29] T. Lu, F. Chen, J Comput Chem 33 (2012) 580–592.
[30] W. Humphrey, A. Dalke, K. Schulten, J Mol Graph 14 (1996) 33–38.
[31] A. Świtlicka, J. Palion-Gazda, B. Machura, J. Cano, F. Lloret, M. Julve, Dalton Trans. 48 (2019) 1404–1417.
[32] A.G. Orpen, L. Brammer, F.H. Allen, O. Kennard, D.G. Watson, R. Taylor, J Chem Soc (1989) S1–S83 Dalton Transactions.
[33] J. Bernstein, R.E. Davis, L. Shimoni, N.L. Chang, Angew. Chem. Int. Ed. 34 (1995) 1555–1573.
[34] M.C. Etter, Acc. Chem. Res. 23 (1990) 120–126.
[35] M.C. Etter, J.C. MacDonald, J. Bernstein, Acta Crystallog. Sec. B 46 (1990) 256–262.
[36] F. Allen, C.A. Baalham, J. Lommerse, P. Raithby, Acta Crystallo Sec. B 54 (1998) 320–329.
[37] E. Espinosa, I. Alkorta, J. Elguero, E. Molins, J Chem Phys 117 (2002) 5529–5542.
[38] S.J. Grabowski, P. Lipkowski, J. Phys. Chem. A 115 (2011) 4765–4773.
[39] S.J. Grabowski, J. Leszczynski, Chem Phys 355 (2009) 169–176.
[40] R.F.W. Bader, Atoms in Molecules: A Quantum Theory, Clarendon Press, 1994.
[41] S.M. Maley, R.C. Mawhinney, J Comput Chem 40 (2019) 916–924.
[42] S. Nanayakkara, E. Kraka, Phys. Chem. Chem. Phys. 21 (2019) 15007–15018.
[43] S. Lee, A.B. Mallik, D.C. Fredrickson, Cryst Growth Des 4 (2004) 279–290.
[44] A. Paul, M. Kubicki, A. Kubas, C. Jelsch, K. Fink, C. Lecomte, J. Phys. Chem. A 115 (2011) 12941–12952.
[45] P. Sharma, A. Gogoi, A.K. Verma, A. Frontera, M.K. Bhattacharyya, New J Chem. 44 (2020) 5473–5488.